LANGMUIR

pubs.acs.org/Langmuir Article

Fabrication of a Postfunctionalizable, Biorepellent, Electroactive Polyurethane Interface on a Gold Surface by Surface-Assisted Polymerization

Sezer Özenler, Yigit Sozen, Hasan Sahin, and Umit Hakan Yildiz*

Cite This: *Langmuir* 2020, 36, 6828–6836 Read Online

ACCESS | Metrics & More | Article Recommendations | Supporting Information

ABSTRACT: This study describes surface-assisted (SurfAst) urethane polymerization, providing a modular/postfunctionalizable, biorepellent, electroactive ∼10 to 100 nm-thick polyurethane (PU) interface on a gold surface. SurfAst is a functionalization methodology based on sequential incubation steps of alkane diisocyanates and alkanediol monomers. The gold surface is functionalized by alkane diisocyanates in the first incubation step, and our theoretical calculations reveal that while the isocyanate group atoms (N, C, and O) at one end of the molecule exhibits strong interactions (∼900 meV) with surface atoms, the other end group remains unreacted. After the first incubation step, sequential alkanediol and alkane diisocyanate incubations provide formation of the PU interface. The extensive analysis of the PU interface has been conducted via X-ray photoelectron spectroscopy, and the chemical mapping verifies that the interface is made of PU moieties. The topographical analysis of the surface conducted by the atomic force microscopy shows that the PU interface consists of mostly a nanoporous texture with 150 nm total roughness. The adherence force mapping of the PU interface reveals that the nanoporous matrix exhibits an adhesion force of about 14 nN. The electrostatic force microscopy characterizing long-range electrostatic interactions (40 nm) shows that the PU interface has been attracted by positively charged species as compared to negative objects. Finally, it is demonstrated that the PU interface is readily postfunctionalizable by polyethylene glycol (PEG 1000), serving as a biorepellent interface and preserving electroactivity. We foresee that SurfAst polymerization will have potential for the facile fabrication of a postfunctionalizable and modular biointerface which might be utilized for biosensing and bioelectronic applications.

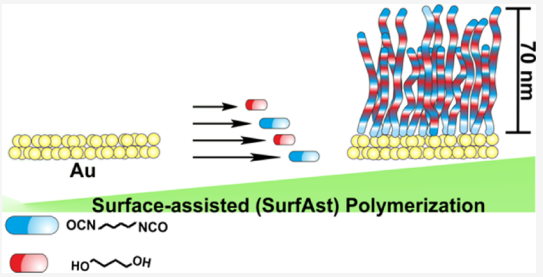

The new-generation biosensors[1,2] and implantable bioelectronic systems[3−5] have become an active research field by growing interactions of humans and machines.[6] Recent advances correspond that the key to the success of the field are mostly related to establishing, preserving, and sustaining delicate balance at the interface between bio- and electronic components.[7] Therefore, the capabilities of interface engineering have been adapted to fabricate soft and stimuli-responsive interface on metals or semiconductors which are the electronic component of bioelectronic systems.[8−13] The major challenge for the functional bioelectronic interface appears to be biofouling caused by irreversible adsorption by bio-macromolecules (proteins and DNAs). Here, "grafting-from" methodologies such as surface-initiated atom transfer radical polymerization (SI-ATRP) and activators regenerated by electron transfer (ARGET) ATRP emerged as a suitable approach to fabricate biorepellent polymer-functionalized surfaces.[14−17] In the last decade, the SI-ATRP methodology has emerged as a useful strategy that provides unique opportunities in surface and interface engineering. Earlier, Pinto et al. have reported the fabrication of gate insulators of low-voltage organic field-effect transistors (OFETs) in which the insulator was made of ultrathin poly methyl methacrylate brushes synthesized via ATRP.[18] Recently, Ge et al. have shown that modulating the Si surface via polymer brushes that were synthesized by SI-ATRP facilitates the fabrication of inkjet-printable OFETs.[19]

In a recent study, Joh et al. have exemplified that Al_2O_3, ZrO_2, and SiO_2 dielectric-layered complementary metal oxide semiconductors were modified by poly(oligo(ethylene glycol) methyl ether methacrylate) brushes. They also showed that polymer brush-modified biosensor platforms exhibit high protein repellency and therefore maximizing performance of sensing devices.[20,21] Last but not least, Tang et al. have presented that poly(oligo(2-alkyl-2-oxazoline)methacrylates)-functionalized gold surfaces were exhibiting good antifouling properties and utilized as the surface plasmon resonance sensor interface.[22] As highlighted in these studies, the laborious degassing steps are a major disadvantage of SI-ATRP that

Received: December 21, 2019
Revised: May 25, 2020
Published: May 27, 2020

https://dx.doi.org/10.1021/acs.langmuir.9b03922
Langmuir 2020, 36, 6828−6836

Scheme 1. SurfAst Polymerization Requires Monomer (HDI) Incubation on Gold at First Step; Then, Consecutive Urethane Condensation Reaction Takes Place between HDI and Second Monomer (1,4-BDO) at the Solution−Substrate Interface; the Multiple Sequential Incubations Yield the PU Layer, and the Final Step Illustrates Post Modification of the PU Layer by PEG

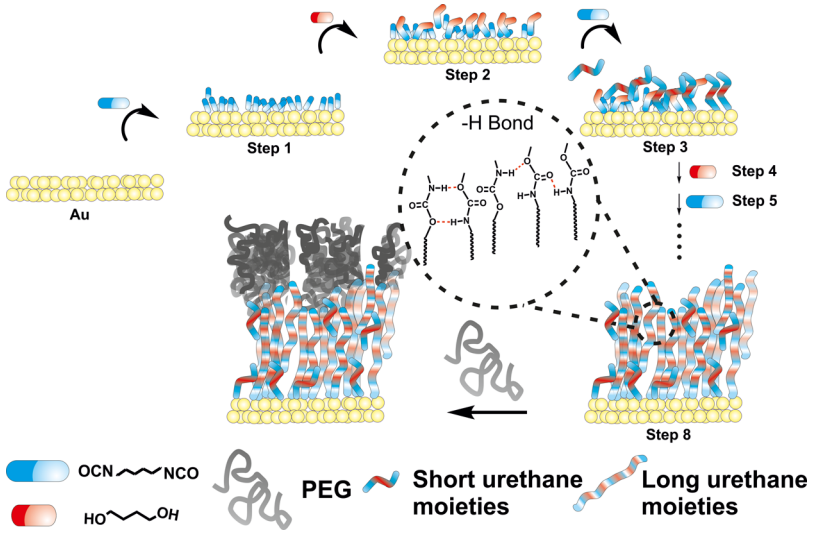

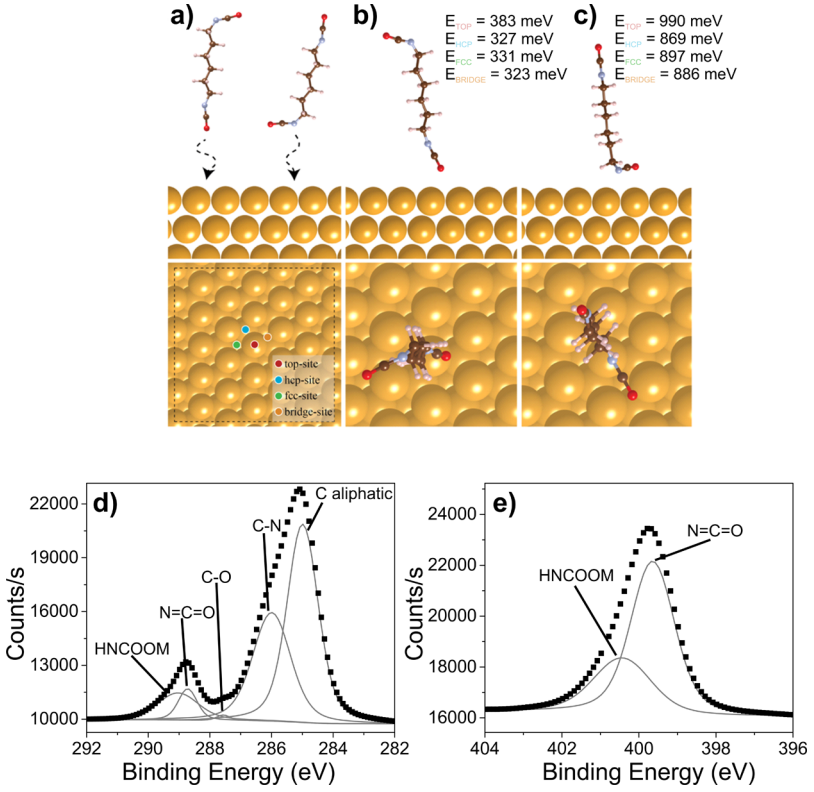

Figure 1. (a) Representative illustration of diffusing HDI molecules with vertically and horizontally aligned NCO atomic groups toward the Au(111) surface. The possible adsorption sites are signified by colored dots in the top view of the Au(111) surface. (b,c) Top and side views of optimized HDI molecules with different NCO orientations against the Au(111) surface and their calculated binding energies for each adsorption site. (d,e) XPS spectra of C 1s and N 1s after HDI incubation.

limits the applicability. On the other hand, air tolerant methodologies are emerging as an alternative approach to SI-ATRP. Yeow et al. have reviewed numerous recent studies that were reporting the pros and cons of air-tolerant controlled living radical polymerization methodologies.[23] Jeong et al. recently presented the air-tolerant SI-ARGET ATRP method for the polymerization of sulfobetaine acrylamide on gold, glass, stainless steel, and ITO surfaces. It is shown that the poly(SBAA)-functionalized gold surfaces exhibit 12−14% protein adsorption.[24] In another study, Hong et al. have shown polymerization of carboxybetaine by SI-ARGET ATRP to fabricate ultralow fouling gold surfaces.[25] Although SI-ATRP and SI-ARGET ATRP methods are effective methodologies to modify the surface of metals, semiconductors, and high dielectric metal oxides, they still require laborious steps of

https://dx.doi.org/10.1021/acs.langmuir.9b03922
Langmuir 2020, 36, 6828−6836

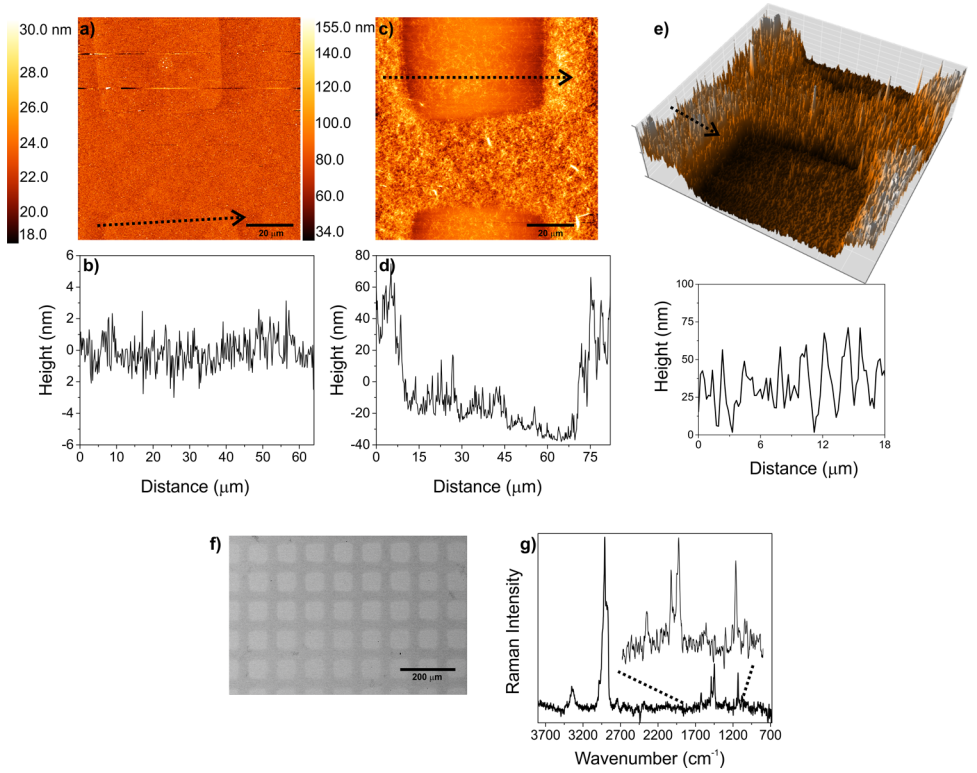

Figure 2. (a,b) AFM height image and profile of 11-mercapto-1-undecanol micropattern-passivated Au; (c,d) AFM height image and profile after eight steps of SurfAst polymerization; (e) 3D chart view of (c) and cross-section (black dashed line); (f) SEM images of SurfAst-modified gold substrate; (g) RAMAN spectrum of the surface inset: magnified view of the fingerprint region.

polymerization which may be considered as disadvantageous for practical biosensing applications.[26]

In this study, we describe surface-assisted (SurfAst) urethane polymerization, yielding a thin polyurethane (PU) interface on the gold surface. This new surface functionalization methodology does not require inert conditions, degassing, or even high-cost catalysts that limit the feasibility.

The SurfAst propagates by sequential incubation steps of substrates in monomer solutions at ambient conditions. The formation of the PU interface by SurfAst polymerization on the gold surface is shown in Scheme 1. The first step is initiated by hexamethylene diisocyanate (HDI) incubation in the presence of the dibutyltin dilaurate (DBTDL) catalyst, providing the isocyanate-functionalized gold surface. Seemingly, isocyanate group atoms (N, C, and O) at both ends of HDI have an equal tendency to interact with the gold surface. Our density functional theory (DFT)-based calculations clearly revealed that adsorption of the HDI molecule through N, C, and O atoms, exhibiting varying potentials on the Au surface.

As shown in Figure 1a, possible adsorption sites were selected which were described as top-site, hcp-site, fcc-site, and bridge-site, to understand how a single HDI molecule is adsorbed by the Au(111) surface. It is considered to be necessary to investigate the effect of NCO orientation on the adsorption characteristics of the HDI molecule to get a clear knowledge between the HDI and Au interface. Therefore, first, the HDI molecule is settled at possible adsorption sites relative to the oxygen atom of the NCO group that aligned vertically on the surface. Later on, the orientation of the NCO group is changed parallel to the surface and positioned on sites relative to the nitrogen atom. According to the calculated binding energies, as represented in Figure 1b,c, the favorable adsorption point is found to be the top-site for each configuration of the HDI molecule. Besides, it is also revealed that the HDI molecule reaches its most favorable energy configuration when the NCO atoms at one end is horizontally aligned to the surface, while the aliphatic chain is positioned perpendicular to the surface. This may be attributed to the tendency of the N atom to interact with the topmost Au atom and followed by collective organization of neighboring aliphatic chains. Here, the high binding energies indicate that much stronger forces exist between the HDI and Au(111) interface than the van der Waals-type weak interactions. Based on DFT results, the N atom at one end of the HDI molecule interacts to the Au surface strongly, while the other end group NCO remains free.[27] The further DFT analysis points out that the bond between N and Au is of partially covalent and metallic character (see Figure S1). After step one, the X-ray photoelectron spectroscopy (XPS) analysis is carried out. The C 1s spectrum, as shown in Figure 1d, deconvoluted into five peaks. The peak at 284.99 eV (FWHM: 1.2) corresponds to C−C aliphatic carbons. Carbon bound to nitrogen (C−N) and C−O is assigned to 285.99 (FWHM: 1.46) and 287.56 eV (FWHM: 0.5), respectively. The peak located at 288.72 eV is assigned to the N═C═O groups (FWHM: 0.72), and the high binding energy peak at 289.03 eV (FWHM: 1.57) is attributed to NHCOOM. In Figure 1e, N 1s spectra are deconvoluted to two peaks at 399.64 (FWHM: 1.35) and 400.43 eV (FWHM: 1.78), corresponding to the N═C═O groups and NHCOOM, respectively.[28,29] These results assure that the Au surface has functionalized by HDI by completion of step one. At the second step, the isocyanate-functionalized gold surface is then incubated with 1,4-butanediol (1,4-BDO) to form a urethane bond. In this study, the resultant PU

https://dx.doi.org/10.1021/acs.langmuir.9b03922
Langmuir 2020, 36, 6828−6836

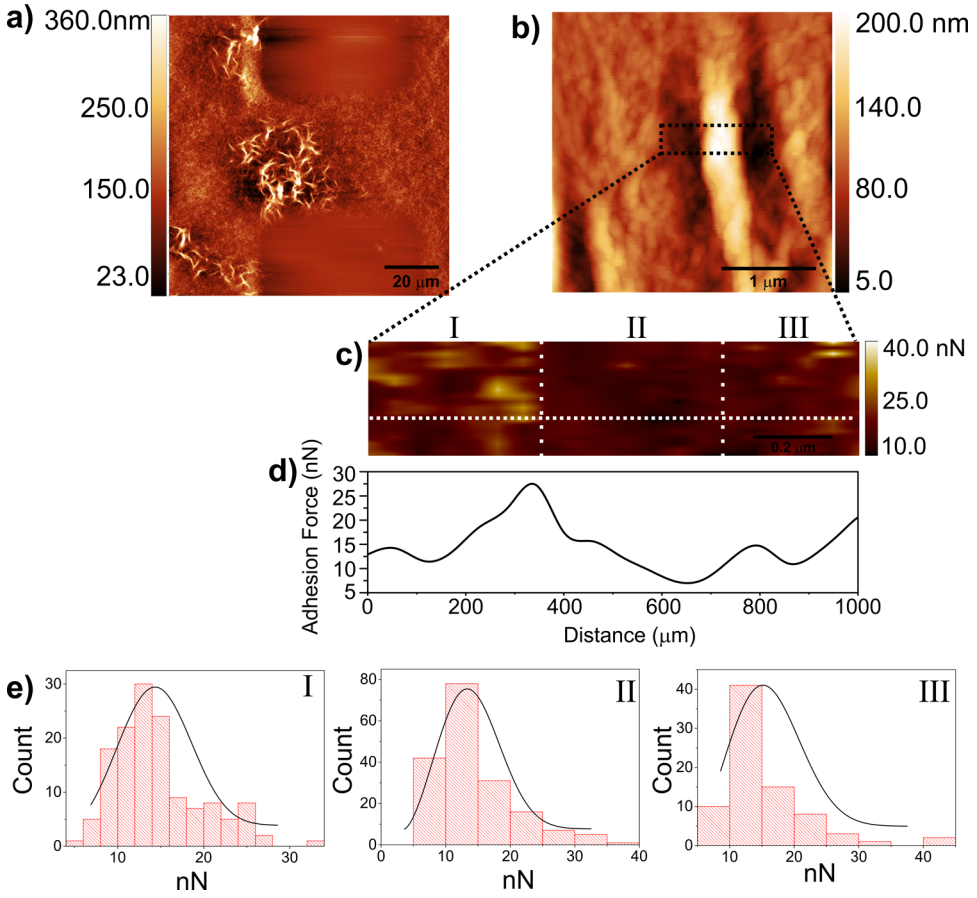

Figure 3. (a,b) AFM images of the nanoporous structure and rodlike domains after SurfAst polymerization; (c) adherence force mapping of the PU interface (rectangle black dashed); (d) adhesion force profile (horizontal white dashed line); and (e) distribution of the adherence force of region I (left), region II (middle), and region III (right).

interface on the gold surface is obtained by eight steps (four sequential condensation reactions; see the schematic 1 for each steps). At the end of the eighth step, a highly mixed hydrogen bonding system potentially is formed that consists of both short and more propagated PU chains. Additionally, free urethane species may bridge the surface-linked PU by assembling more chains through strong hydrogen bonding.

Figure 2a,c shows the gold surface before and after SurfAst polymerization reactions. Prior to SurfAst polymerization, the gold surface was passivated (micropatterned) by 11-mercapto-1-undecanol to facilitate determination of thickness via atomic force microscopy (AFM). In Figure 2a, the height image of the 11-mercapto-1-undecanol-passivated gold surface is shown; the average height distribution of 2.5 nm was found (Figure 2b). This height distribution (2.5 nm) refers to the perfect packing of 11-mercapto-1-undecanol molecules that may avoid non-specific interaction of diisocyanate by the passivated surface. Figure 2c shows the AFM image of the gold surface after eight steps of incubations (four sequential reactions between 1,4-BDO and HDI). As seen in this figure, the PU interface has characteristic nanoporous structures and is homogeneously distributed with a sharp border pattern on the gold surface. The average height distribution of the PU interface at the nonpassivated area was found to be ∼70 nm (height profile shown in Figure 2d). The formation of the nanoporous structure may be attributed to stimulated hydrogen bonding between urethane chains which provide collective interchain interactions. The 3D map presented in Figure 2e shows topography of the nanoporous structure, and the height profile reveals that average surface roughness is 150 nm.

The scanning electron microscopy (SEM) image of the gold surface (Figure 2f) reveals that the nanoporous structure is homogenously distributed in a large area. It has been found that at least eight steps are required to obtain the nanoporous structure interface in the SurfAst polymerization. This result shows that PU functionalization by SurfAst polymerization may accomplish a perfect interface nearly 0.25 cm^2 area. Moreover, the light microscopy images, as shown in Figure S3, demonstrate that the large-area interface was readily provided by SurfAst polymerization. The functional group analysis has been performed by Raman and Fourier-tranform infrared (FTIR) spectroscopies. The Raman spectra of the surface, as shown in Figure 2g, demonstrate asymmetric aliphatic C−H stretching at 2907 cm^{-1}, symmetric stretching at 2873 cm^{-1}, C−H bending vibration band at 1445 cm^{-1}, and CHN group vibration at 1490 cm^{-1}. Hydrogen bond-associated secondary urethane (−HN−CO−O−) N−H stretching was found at ca. 3330 cm^{-1} and secondary amide C═O stretching (solid phase) at ca. 1625 cm^{-1}. The peak observed at 1130 cm^{-1} was assigned to urethane-attached C−H deformation.[30,31] The Raman spectrum verifies that the nanoporous structure was made of urethane bonds. As pointed out by Kojio et al., the FTIR investigation of thin PU films exhibits two characteristic peaks at 1704 and 1730 cm^{-1} that are assigned to the hydrogen-bonded carbonyl stretching band and free one, respectively.[32] We have also conducted FTIR characterization

https://dx.doi.org/10.1021/acs.langmuir.9b03922
Langmuir 2020, 36, 6828−6836

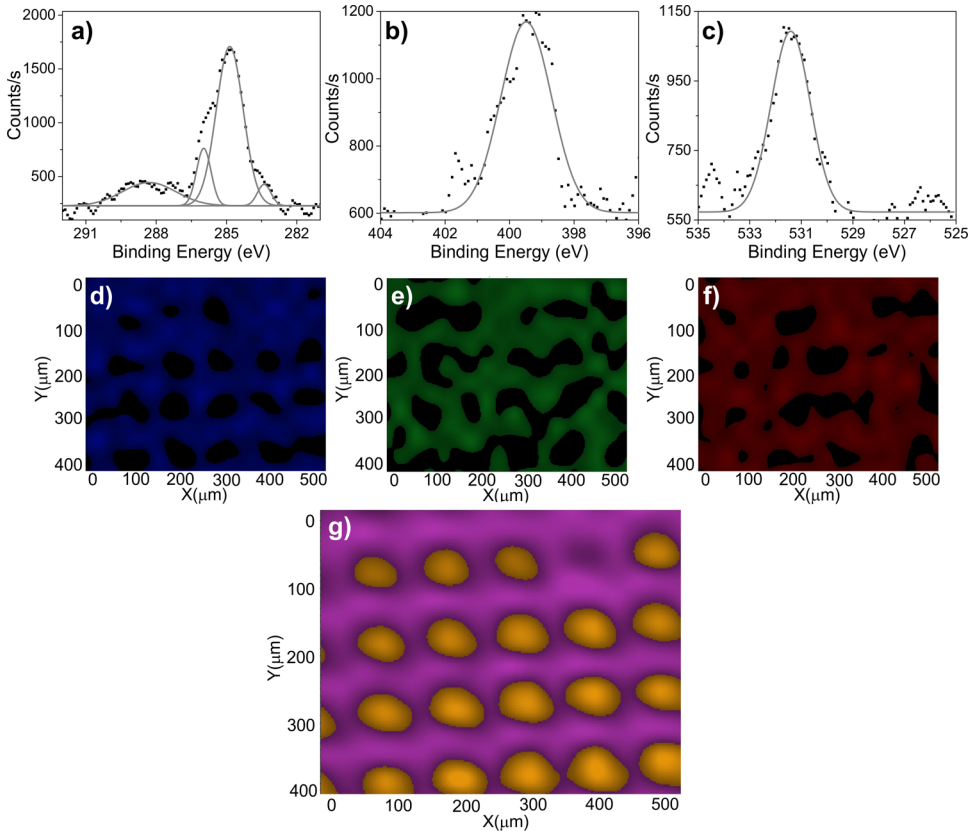

Figure 4. (a) XPS spectra of (a) C 1s, (b) N 1s, and (c) O 1s chemical mapping results of (d) C 1s, (e) N 1s, and (f) O 1s after SurfAst polymerization; (g) XPS chemical mapping of the PU interface.

of our PU interfaces (see Figure S5) that shows two characteristic peaks at 1734 and 1699 cm^{-1}. The peak intensities at 1699 cm^{-1} slightly decrease as the number of steps increases, referring to hydrogen-bonded carbonyl stretching marginally decreasing. In general, the five absorption bands are observed nearly at 1740 and 1730 cm^{-1} for free carbonyls and 1725, 1713, and 1702 cm^{-1} for hydrogen-bonded carbonyls.[33,34] The remaining three peaks were assigned at 1708 and 1718 cm^{-1} for hydrogen-bonded carbonyl, and 1750 cm^{-1} bands for free carbonyl. In particular, 1708 cm^{-1}, NH···O−C, and 1718 cm^{-1}, binary NH···O−C, was assigned to hydrogen bonds between the hard segments. These results show that there are at least three types of hydrogen bonds in the structure (see the Supporting information S5). We concluded that the presence of hydrogen-bonded carbonyls may be attributed to the interacting urethane moieties.

Here, we concluded that the yield of SurfAst polymerization reaction depends on the increasing number of incubations. At initial steps, (up to step three), the surface may be supersaturated by adsorption of the monomers; therefore, low-molecular weight oligo−urethanes are formed, yielding a low height profile. Contrary to initial steps, between sixth to eighth steps, the urethane condensation reaction yields polymer at the interface and therefore exhibits a 70 nm height profile.

The AFM characterization shows that the nanoporous structure exhibits some heterogeneous rodlike domains. In Figure 3a,b, the AFM image of the PU interface reveals rodlike domains besides the nanoporous structure. The formation of rodlike domains may be attributed to parallel stacking of urethane groups via hydrogen bonding between neighboring C═O···H−N. As reported by Check et al., a linear molecular structure of urethane monomers induces such parallel stacking.[35] Mishra et al. had also reported that linear isocyanate-containing PU exhibits microcluster structures made of parallel stacking of urethane groups.[36] As explained earlier by Yilgör et al., the symmetry of urethane monomers (HDI/BDO) contributes to the strong interaction of hard segment contents, thereby increasing hydrogen bond strength. Therefore, we assume that the symmetry of urethane monomers contributes the formation of rodlike domains.[37,38] The rodlike domains in the PU interface may be considered as heterogeneous domains that may influence interfacial properties. Therefore, to understand the effect of rod and nanoporous structures on interface properties such as the antifouling property, adherence force measurements have been performed. Figure 3c shows adherence force mapping of the PU interface including both rodlike domains and nanoporous structure. The adhesion value of the rodlike domains is 13.30 nN and for the nanoporous structures, it is 14.36 nN (Figure 3d,e). This result assures that the nanoporous structure exhibits a uniform adhesion profile through some structural inhomogeneities such as rodlike domains.

XPS analysis was performed to obtain the binding energies and chemical mapping of the PU nanoporous structure on the gold surface. The C 1s spectrum is shown in Figure 4a. C−(C−H) species at 284.8 eV are dominant, and the minor peak at 283.5 eV is present; 286.0 eV corresponds to ether carbon C−O(C═O), 288.35 eV refers to the N−(C═O)−O carbamate group. The N 1s spectrum exhibits a sharp peak at 399.4 eV (O═C)−N (Figure 4b), while the O 1s spectrum

https://dx.doi.org/10.1021/acs.langmuir.9b03922
Langmuir 2020, 36, 6828−6836

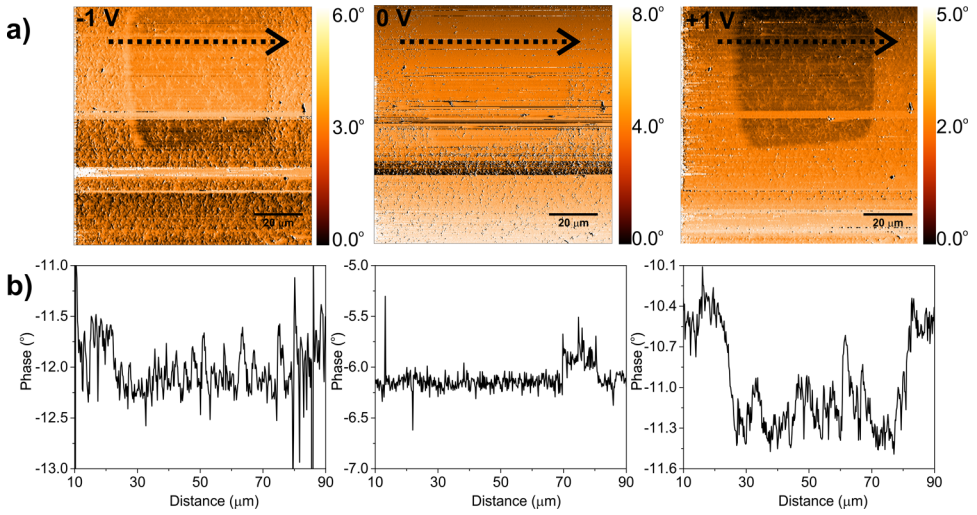

Figure 5. (a) EFM image after SurfAst polymerization with −1, 0 and +1 V, respectively; (b) phase-shift profiles.

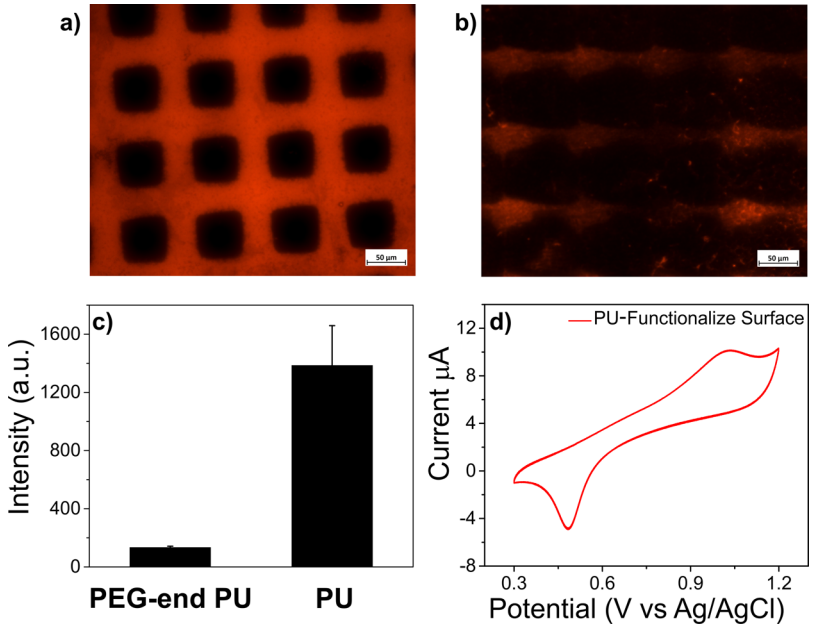

Figure 6. (a) Fluorescence image of the PU-functionalized surface with Texas Red-conjugated bovine serum albumin (BSA-T) adsorption of PU; (b) PEG-end PU-functionalized surface; (c) fluorescence intensity of PU and PEG-end PU-functionalized surface; (d) cyclic voltammogram of bare gold and PU-functionalized surface measured against Ag/AgCl (3 M KCl) (scan rate: 10 mV/s to 0.01 M phosphate buffer (pH: 6.8)—1 mM $K_4Fe(CN)_6$).

shows a peak at 531.4 eV (FWHM: 1.24 eV), corresponding to group C−(C═O)−O; the peak broadening toward higher energy (532.5 eV) may refer to ether oxygen in C−(C═O)−O in Figure 4c.[39−41] XPS chemical mapping of the PU interface is shown in Figure 4d−f results (500 × 400 μm) blue, green, and red regions refer to the sum concentration distributions of C 1s, N 1s, and O 1s of the PU interface on the gold surface. The chemical abundance of carbon, oxygen, and nitrogen was analyzed based on the ratio of black to colored regions, and it demonstrates that carbon was found to be the most abundant on the surface as compared to oxygen and nitrogen. As shown in Figure 4g, XPS chemical mapping is consistent with AFM topography mapping, and this result proves that the nanoporous structure is made from PU.

The electrostatic interactions are assumed to be long-range interactions that play a pivotal role in the case of protein adsorption. Here, we aimed to mimic the attraction profile of a charged object (protein) by the nanoporous surface. Therefore, we performed electrostatic force microscopy (EFM) imaging, as shown in Figure 5a to monitor the electrostatic interactions between charged species and nanoporous surfaces. The EFM tip has been positioned above 40 nm to the PU surface and charged by applying 0, +1, and −1 V. Figure 5b represents the EFM (phase shift) measurement for three different voltages applied to the tip. In Figure 5b, V_{tip} is set to −1 V, causing a 0.49° phase shift between the polymer and gold layer. When V_{tip} is set to +1 V, it results in a 1.57° phase shift between the polymer and gold layer. These results demonstrate that positively charged species prone to interact with the surface because they induce long-range electrostatic interactions as compared to negatively charged species.[42]

https://dx.doi.org/10.1021/acs.langmuir.9b03922
Langmuir 2020, 36, 6828−6836

The XPS and AFM results prove that surfAst polymerization yields uniform PU made up of the nanoporous interface which provide homogeneous surface properties in large areas. The methodology described here shows that nanoporous PU may be designed as a postfunctionalizable interface and may serve as a modular platform depending on end use. As a proof of this concept, we have shown the postfunctionalization of polyethylene glycol (PEG 1000) on PU. Figure S9 shows the attenuated total reflection spectra prior and post modification of PEG, exhibiting an increase in intensity of C−O−C stretching at 1100 cm^{-1} and decrease in intensity of NCO stretching at 2250 cm^{-1}. The yield of PEG functionalization was found to be ∼30% (calculation details are given in the Supporting Information section). This result refers to accomplishment of PEG functionalization. Figure 6a is the fluorescence image of the PU-coated surface after incubation with BSA-T. It demonstrated that uniform protein adherence occurs on the PU interface. In contrast, after PEG functionalization, a significant drop in fluorescence intensity of BSA-T has been observed (Figure 6b) which proves the efficient functionalization of the PEG layer on PU. As shown in Figure 6c, the total fluorescence intensity has been lowered nearly 10 folds by the PEG-end PU surface. This result demonstrated that postfunctionalization of the PU interface has been accomplished, and the PEG layer exhibits an efficient protein repellent property. Finally, we have conducted cyclic voltammetry measurements for the PEG-end PU surface; Figure 6d shows the electroactivity of the PU-functionalized surface, where PU thickness is about 70 nm; it displays 11 μA of peak current. It assures that the PU-functionalized Au surface is electroactive.

In summary, we have demonstrated that a novel gold functionalization methodology named SurfAst urethane polymerization is suitable for utilization of the nanoporous polymer interface on a solid substrate. The described methodology provides a postfunctionalizable, modular ∼10 to 100 nm-thick PU interface on the gold surface. The PU interface consists of nanoporous structures with some rodlike domains. EFM monitoring has showed that the PU interface was found to be more attractive by positively charged species as compared to negatively charged species. We also demonstrated that the nanoporous PU interface was postfunctionalizable by PEG and served as the protein repellent surface. The methodology is holding a great promise of easy fabrication of an electroactive, antifouling biointerface. In this study, we described the PU interface on the gold surface obtained by the SurfAst polymerization method, but further studies on the other noble-metal and high-κ metal oxide surfaces are ongoing.

EXPERIMENTAL SECTION

11-Mercapto-1-undecanol, poly(ethylene glycol) (Mw: 1000 Da), 1,4-BDO, HDI, acetone, and DBTDL 95% were purchased from Sigma-Aldrich and used as received without further purification. T-BSA was purchased from Thermo Fisher.

Theoretical Calculations. The adsorption of the HDI molecule on the Au(111) surface is investigated by carrying out the DFT method conducted in the Vienna Ab initio Simulation Package (VASP)[43,44] related to projector augmented wave[45] pseudopotentials. Exchange−correlation energy of the system is approximated by the generalized gradient approximation functional developed by Perdew−Burke−Ernzerhof,[46] and weak dispersion forces are corrected by including the DFT-D2 method of Grimme[47] that enables to identify more accurate correlation energies. Cut-off energy for the plane−wave basis set is limited with 500 eV, and the 2 × 2 × 1 k-point mesh is found to be efficient to integrate the Brillouin zone of the system. Partial occupancies are determined according to the Gaussian smearing method which smears the Fermi level with a width of 0.05 eV. For a realistic model of the Au(111) surface, a rectangular conventional cell is constructed, cutting the unit cell of the bulk Au crystal from the (111) lattice plane. Later on, the created unit cell is enlarged to a 5 × 3 × 1 supercell, and the vacuum spacing along the z-direction is increased to 30 Å to avoid the neighboring interactions in adsorption calculations. Before structural relaxations, the HDI molecule is settled 2.5 Å above from the topmost layer of the relaxed Au(111) surface. After the structural optimization of the HDI−Au(111) system, binding energies are calculated by using the equation $E_{binding} = E_{HDI} + E_{surface} - E_{HDI+Au(111)}$. While E_{HDI} and $E_{surface}$ stand for the total energies of the bare Au(111) surface and HDI molecule, $E_{HDI+Au(111)}$ stand for the total energy of the HDI + Au(111) system.

Atomic Force Spectroscopy. Nanosurf AFM (Stat0.2LAuD, static force) was used for topographical characterization of gold surfaces. Electrostatic force microscopy was employed to characterize the electrostatic behavior of PU interface. The EFM measurement was conducted in contour mode (tip altitude was fixed 40 nm above from the surface), at ambient temperature. The data analysis of nanomechanical characterization was conducted from 0.25 μm^2 region by SPIP 6.7.8 and AtomicJ software. The surface morphology of the gold surfaces was examined by using the Quanta 250 FEG scanning electron microscope.

Raman spectra (MonoVista-Princeton Instruments) were recorded in a spectral range between 700 and 3700 cm^{-1} using 532 nm laser to observe PU functional groups on the gold surface. The measurements were taken in combination with a 100× microscope objective.

X-ray Photoelectron Spectroscopy. XPS mapping analyses (500 × 400 μm) were performed at a pass energy of 30 eV. An Al Kα monochromatic (1486.68 eV) beam was used with a spot size of 30 μm (3 number of scans). XPS point analyses were conducted with 400 μm spot size. The gold surface is prepared by the following procedure: HDI (160 mM) and DBTDL (90 × 10^{-3} mM) were dissolved in the 2 mL acetone solution. The gold surface was incubated in acetone at 40 °C for 30 min. After incubation, the gold was sonicated with acetone thoroughly three times.

Gold Surface Preparation. Gold (Au) substrates (1 cm^2) were cleaned by the RCA cleanser that contains deionized water (DI), 30% hydrogen peroxide, and 27% ammonium hydroxide (5:1:1 per volume) at 80 °C for 30 min. Gold surfaces were rinsed with excess DI water and dried by N_2 blowing.

11-Mercapto-1-undecanol was used for gold surface passivation. Polydimethylsiloxane stamp was incubated in 1 mM 11-mercapto-1-undecanol in ethanolic solution for 5 min. The stamp was dried by a jet of nitrogen. The stamp was placed on the gold surface by applying slight pressure to ensure good contact and passivated to the surface. The stamp remained in contact for 5 min, and the gold surface was rinsed with plenty of EtOH (Figure S10).[48]

SurfAst Urethane Polymerization. Generally, SurfAst polymerization was carried out by the dip-coating process after passivation with 11-mercapto-1-undecanol on the gold surface for the determination of thickness via AFM. 1,4-BDO and HDI concentrations were prepared equimolar (80 mM) in the acetone solutions. DBTDL (4.5 × 10^{-2} mM) was used as the catalyst in the PU reaction. The functionalized gold was incubated with HDI in acetone at 40 °C for 20 min. After every incubation step, the gold was sonicated with acetone thoroughly three times. Then, gold was incubated with 1,4-BDO in acetone at 40 °C for 20 min. Also, at the end of the eighth step, the theoretical molecule length was calculated to be around 9 nm (see Figure S11).

Protein Absorption Assay. PEG 1000 was added to the top of the layer of 1,4-BDO/HDI to further investigate the effect of PEG 1000 on the hydrophilicity property of a gold surface that can be tailored in a controlled manner. After passivated with 11-mercapto-1-undecanol, 1,4-BDO/HDI SurfAst polymerization was carried out on the gold surface. PEG 1000 reacted with HDI at the end of the fourth

https://dx.doi.org/10.1021/acs.langmuir.9b03922
Langmuir 2020, 36, 6828−6836

step to enlighten the effect of PEG (PEG 1000) on antifouling properties.

PEG-end PU and PU-end gold surfaces were incubated with BSA-T in 1 mg/mL concentration in 1× PBS for 3 h at room temperature. After incubation, the gold surfaces were rinsed five times with 1× PBS. Fluorescence imaging of the gold surfaces was performed using Zeiss fluorescence microscopy with an exciting wavelength of 541 nm.

■ ASSOCIATED CONTENT

Supporting Information

The Supporting Information is available free of charge at https://pubs.acs.org/doi/10.1021/acs.langmuir.9b03922.

Light microscope image, additional AFM images, RAMAN microscope image, and XPS survey data (PDF)

■ AUTHOR INFORMATION

Corresponding Author

Umit Hakan Yildiz − *Department of Chemistry, Izmir Institute of Technology, 35430 Izmir, Turkey;* orcid.org/0000-0002-6922-4454; Email: hakanyildiz@iyte.edu.tr; Fax: +90 232 750 7509

Authors

Sezer Özenler − *Department of Chemistry, Izmir Institute of Technology, 35430 Izmir, Turkey;* orcid.org/0000-0001-6045-7035

Yigit Sozen − *Department of Photonics, Izmir Institute of Technology, 35430 Izmir, Turkey*

Hasan Sahin − *Department of Photonics, Izmir Institute of Technology, 35430 Izmir, Turkey;* orcid.org/0000-0002-6189-6707

Complete contact information is available at: https://pubs.acs.org/10.1021/acs.langmuir.9b03922

Notes

The authors declare no competing financial interest.

■ ACKNOWLEDGMENTS

This study has been supported by the IZTECH-Scientific Research Project (2019-IYTE-291) and The Scientific and Technological Research Council of Turkey, TUBİTAK Project: 117F243. Author S.Ö. is a YÖK 100/2000 scholarship holder. XPS chemical mapping was conducted at Ege University Central Research Testing and Analysis Laboratory Research and Application Center (EGE-MATAL). The SEM micrographs were obtained at Material Research (IZTECH-MAM). We are thankful to Nanosurf Company and Terralab Turkiye for their continuous technical support.

■ REFERENCES

(1) Gong, S.; Lai, D. T. H.; Su, B.; Si, K. J.; Ma, Z.; Yap, L. W.; Guo, P.; Cheng, W. Highly Stretchy Black Gold E-Skin Nanopatches as Highly Sensitive Wearable Biomedical Sensors. *Adv. Electron. Mater.* **2015**, *1*, 1400063.

(2) Lee, H.; Hong, Y. J.; Baik, S.; Hyeon, T.; Kim, D.-H. Enzyme-Based Glucose Sensor: From Invasive to Wearable Device. *Adv. Healthc. Mater.* **2018**, *7*, 1701150.

(3) Choi, S.; Han, S. I.; Jung, D.; Hwang, H. J.; Lim, C.; Bae, S.; Park, O. K.; Tschabrunn, C. M.; Lee, M.; Bae, S. Y.; Yu, J. W.; Ryu, J. H.; Lee, S.-W.; Park, K.; Kang, P. M.; Lee, W. B.; Nezafat, R.; Hyeon, T.; Kim, D.-H. Highly conductive, stretchable and biocompatible Ag-Au core-sheath nanowire composite for wearable and implantable bioelectronics. *Nat. Nanotechnol.* **2018**, *13*, 1048−1056.

(4) Lee, S.; Inoue, Y.; Kim, D.; Reuveny, A.; Kuribara, K.; Yokota, T.; Reeder, J.; Sekino, M.; Sekitani, T.; Abe, Y.; Someya, T. A strain-absorbing design for tissue−machine interfaces using a tunable adhesive gel. *Nat. Commun.* **2014**, *5*, 5898.

(5) Xu, L.; Gutbrod, S. R.; Bonifas, A. P.; Su, Y.; Sulkin, M. S.; Lu, N.; Chung, H.-J.; Jang, K.-I.; Liu, Z.; Ying, M.; Lu, C.; Webb, R. C.; Kim, J.-S.; Laughner, J. I.; Cheng, H.; Liu, Y.; Ameen, A.; Jeong, J.-W.; Kim, G.-T.; Huang, Y.; Efimov, I. R.; Rogers, J. A. 3D multifunctional integumentary membranes for spatiotemporal cardiac measurements and stimulation across the entire epicardium. *Nat. Commun.* **2014**, *5*, 3329.

(6) Lim, S.; Son, D.; Kim, J.; Lee, Y. B.; Song, J.-K.; Choi, S.; Lee, D. J.; Kim, J. H.; Lee, M.; Hyeon, T.; Kim, D.-H. Transparent and Stretchable Interactive Human Machine Interface Based on Patterned Graphene Heterostructures. *Adv. Funct. Mater.* **2015**, *25*, 375−383.

(7) Miyamoto, A.; Lee, S.; Cooray, N. F.; Lee, S.; Mori, M.; Matsuhisa, N.; Jin, H.; Yoda, L.; Yokota, T.; Itoh, A.; Sekino, M.; Kawasaki, H.; Ebihara, T.; Amagai, M.; Someya, T. Inflammation-free, gas-permeable, lightweight, stretchable on-skin electronics with nanomeshes. *Nat. Nanotechnol.* **2017**, *12*, 907−913.

(8) Gong, S.; Schwalb, W.; Wang, Y.; Chen, Y.; Tang, Y.; Si, J.; Shirinzadeh, B.; Cheng, W. A wearable and highly sensitive pressure sensor with ultrathin gold nanowires. *Nat. Commun.* **2014**, *5*, 3132.

(9) Lipomi, D. J.; Vosgueritchian, M.; Tee, B. C.-K.; Hellstrom, S. L.; Lee, J. A.; Fox, C. H.; Bao, Z. Skin-like pressure and strain sensors based on transparent elastic films of carbon nanotubes. *Nat. Nanotechnol.* **2011**, *6*, 788−792.

(10) Park, J.; Choi, S.; Janardhan, A. H.; Lee, S.-Y.; Raut, S.; Soares, J.; Shin, K.; Yang, S.; Lee, C.; Kang, K.-W.; Cho, H. R.; Kim, S. J.; Seo, P.; Hyun, W.; Jung, S.; Lee, H.-J.; Lee, N.; Choi, S. H.; Sacks, M.; Lu, N.; Josephson, M. E.; Hyeon, T.; Kim, D.-H.; Hwang, H. J. Electromechanical cardioplasty using a wrapped elasto-conductive epicardial mesh. *Sci. Transl. Med.* **2016**, *8*, 344ra86.

(11) Son, D.; Lee, J.; Qiao, S.; Ghaffari, R.; Kim, J.; Lee, J. E.; Song, C.; Kim, S. J.; Lee, D. J.; Jun, S. W.; Yang, S.; Park, M.; Shin, J.; Do, K.; Lee, M.; Kang, K.; Hwang, C. S.; Lu, N.; Hyeon, T.; Kim, D.-H. Multifunctional wearable devices for diagnosis and therapy of movement disorders. *Nat. Nanotechnol.* **2014**, *9*, 397−404.

(12) Wang, J.; Zhao, X.; Li, J.; Kuang, X.; Fan, Y.; Wei, G.; Su, Z. Electrostatic Assembly of Peptide Nanofiber-Biomimetic Silver Nanowires onto Graphene for Electrochemical Sensors. *ACS Macro Lett.* **2014**, *3*, 529−533.

(13) Weng, Y.-H.; Xu, L.-T.; Chen, M.; Zhai, Y.-Y.; Zhao, Y.; Ghorai, S. K.; Pan, X.-H.; Cao, S.-H.; Li, Y.-Q. In Situ Monitoring of Fluorescent Polymer Brushes by Angle-Scanning Based Surface Plasmon Coupled Emission. *ACS Macro Lett.* **2019**, *8*, 223−227.

(14) Conzatti, G.; Cavalie, S.; Combes, C.; Torrisani, J.; Carrere, N.; Tourrette, A. PNIPAM grafted surfaces through ATRP and RAFT polymerization: Chemistry and bioadhesion. *Colloids Surf., B* **2017**, *151*, 143−155.

(15) Murugan, P.; Krishnamurthy, M.; Jaisankar, S. N.; Samanta, D.; Mandal, A. B. Controlled decoration of the surface with macromolecules: polymerization on a self-assembled monolayer (SAM). *Chem. Soc. Rev.* **2015**, *44*, 3212−3243.

(16) Ngo, B. K. D.; Grunlan, M. A. Protein Resistant Polymeric Biomaterials. *ACS Macro Lett.* **2017**, *6*, 992−1000.

(17) Rodriguez, K. J.; Gajewska, B.; Pollard, J.; Pellizzoni, M. M.; Fodor, C.; Bruns, N. Repurposing Biocatalysts to Control Radical Polymerizations. *ACS Macro Lett.* **2018**, *7*, 1111−1119.

(18) Pinto, J. C.; Whiting, G. L.; Khodabakhsh, S.; Torre, L.; Rodríguez, A.; Dalgliesh, R. M.; Higgins, A. M.; Andreasen, J. W.; Nielsen, M. M.; Geoghegan, M.; Huck, W. T. S.; Sirringhaus, H. Organic Thin Film Transistors with Polymer Brush Gate Dielectrics Synthesized by Atom Transfer Radical Polymerization. *Adv. Funct. Mater.* **2008**, *18*, 36−43.

(19) Ge, F.; Wang, X.; Zhang, Y.; Song, E.; Zhang, G.; Lu, H.; Cho, K.; Qiu, L. Modulating the Surface via Polymer Brush for High-Performance Inkjet-Printed Organic Thin-Film Transistors. *Adv. Electron. Mater.* **2017**, *3*, 1600402.

(20) Joh, D. Y.; McGuire, F.; Abedini-Nassab, R.; Andrews, J. B.; Achar, R. K.; Zimmers, Z.; Mozhdehi, D.; Blair, R.; Albarghouthi, F.; Oles, W.; Richter, J.; Fontes, C. M.; Hucknall, A. M.; Yellen, B. B.; Franklin, A. D.; Chilkoti, A. Poly(oligo(ethylene glycol) methyl ether methacrylate) Brushes on High-κ Metal Oxide Dielectric Surfaces for Bioelectrical Environments. *ACS Appl. Mater. Interfaces* **2017**, *9*, 5522−5529.
(21) Ma, H.; Hyun, J.; Stiller, P.; Chilkoti, A. "Non-Fouling" Oligo(ethylene glycol)- Functionalized Polymer Brushes Synthesized by Surface-Initiated Atom Transfer Radical Polymerization. *Adv. Mater.* **2004**, *16*, 338−341.
(22) Tang, P.; di Cio, S.; Wang, W.; Gautrot, J. Surface-Initiated Poly(oligo(2-alkyl-2-oxazoline)methacrylate) Brushes. *Langmuir* **2018**, *34*, 10019−10027.
(23) Yeow, J.; Chapman, R.; Gormley, A. J.; Boyer, C. Up in the air: oxygen tolerance in controlled/living radical polymerisation. *Chem. Soc. Rev.* **2018**, *47*, 4357−4387.
(24) Jeong, W.; Kang, H.; Kim, E.; Jeong, J.; Hong, D. Surface-Initiated ARGET ATRP of Antifouling Zwitterionic Brushes Using Versatile and Uniform Initiator Film. *Langmuir* **2019**, *35*, 13268−13274.
(25) Hong, D.; Hung, H.-C.; Wu, K.; Lin, X.; Sun, F.; Zhang, P.; Liu, S.; Cook, K. E.; Jiang, S. Achieving Ultralow Fouling under Ambient Conditions via Surface-Initiated ARGET ATRP of Carboxybetaine. *ACS Appl. Mater. Interfaces* **2017**, *9*, 9255−9259.
(26) Zoppe, J. O.; Ataman, N. C.; Mocny, P.; Wang, J.; Moraes, J.; Klok, H.-A. Surface-Initiated Controlled Radical Polymerization: State-of-the-Art, Opportunities, and Challenges in Surface and Interface Engineering with Polymer Brushes. *Chem. Rev.* **2017**, *117*, 1105−1318.
(27) Fug, F.; Nies, C.; Possart, W. in situ FTIR study of adhesive interactions of 4,4′-methylene diphenyl diisocyanate and native metals. *Int. J. Adhes. Adhes.* **2014**, *52*, 66−76.
(28) Beamson, G. *High Resolution XPS of Organic Polymers: The Scienta ESCA 300 Database*; John Wiley & Sons, 1992.
(29) Tardio, S.; Abel, M.-L.; Carr, R. H.; Watts, J. F. The interfacial interaction between isocyanate and stainless steel. *Int. J. Adhesion Adhes.* **2019**, *88*, 1−10.
(30) Lin-Vien, D.; Colthup, N. B.; Fateley, W. G.; Grasselli, J. G. *The Handbook of Infrared and Raman Characteristic Frequencies of Organic Molecules*; Academic Press, 1991.
(31) Socrates, G. *Infrared and Raman Characteristic Group Frequencies: Tables and Charts*, 3rd ed; Wiley, 2004; p 366.
(32) Kojio, K.; Uchiba, Y.; Mitsui, Y.; Furukawa, M.; Sasaki, S.; Matsunaga, H.; Okuda, H. Depression of Microphase-Separated Domain Size of Polyurethanes in Confined Geometry. *Macromolecules* **2007**, *40*, 2625.
(33) Strikovsky, A. G.; Zharkov, V. V.; Letunovsky, M. P. Ir-spectroscopy of hydrogen bond as a method of analytical determination of physical network in poly(ether urethane)s. *Macromol. Symp.* **1995**, *94*, 181−188.
(34) Zharkov, V. V.; Strikovsky, A. G.; Verteletskaya, T. E. Amide I absorption band: description of the urethane group association scheme in polyether urethane elastomers. *Polymer* **1993**, *34*, 938−941.
(35) Check, C.; Imre, B.; Gojzewski, H.; Chartoff, R.; Vancso, G. J. Kinetic aspects of formation and processing of polycaprolactone polyurethanes in situ from a blocked isocyanate. *Polym. Chem.* **2018**, *9*, 1983−1995.
(36) Mishra, A.; Aswal, V. K.; Maiti, P. Nanostructure to Microstructure Self-Assembly of Aliphatic Polyurethanes: The Effect on Mechanical Properties. *J. Phys. Chem. B* **2010**, *114*, 5292−5300.
(37) Klinedinst, D. B.; Yilgör, E.; Yilgör, I.; Beyer, F. L.; Wilkes, G. L. Structure-property behavior of segmented polyurethaneurea copolymers based on an ethylene-butylene soft segment. *Polymer* **2005**, *46*, 10191−10201.
(38) Yilgör, I.; Yilgör, E.; Wilkes, G. L. Critical parameters in designing segmented polyurethanes and their effect on morphology and properties: A comprehensive review. *Polymer* **2015**, *58*, A1−A36.
(39) Queiroz, D.; Botelhodorego, A.; Depinho, M. Bi-soft segment polyurethane membranes: Surface studies by X-ray photoelectron spectroscopy. *J. Membr. Sci.* **2006**, *281*, 239−244.
(40) Shimizu, K.; Phanopoulos, C.; Loenders, R.; Abel, M.-L.; Watts, J. F. The characterization of the interfacial interaction between polymeric methylene diphenyl diisocyanate and aluminum: a ToF-SIMS and XPS study. *Surf. Interface Anal.* **2010**, *42*, 1432−1444.
(41) Vargo, T. G.; Hook, D. J.; Gardella, J. A.; Eberhardt, M. A.; Meyer, A. E.; Baier, R. E. A Surface Spectroscopic and Wettability Study of a Segmented Block Copolymer Poly(etherurethane). *Appl. Spectrosc.* **1991**, *45*, 448−456.
(42) El Khoury, D. Towards the use of Electrostatic Force Microscopy to study interphases in nanodielectric materials. Ph.D. Thesis, Université de Montpellier, 2017.
(43) Kresse, G.; Furthmüller, J. Efficient iterative schemes forab initiototal-energy calculations using a plane-wave basis set. *Phys. Rev. B: Condens. Matter Mater. Phys.* **1996**, *54*, 11169−11186.
(44) Kresse, G.; Hafner, J. Ab initiomolecular dynamics for liquid metals. *Phys. Rev. B: Condens. Matter Mater. Phys.* **1993**, *47*, 558−561.
(45) Blöchl, P. E. Projector augmented-wave method. *Phys. Rev. B: Condens. Matter Mater. Phys.* **1994**, *50*, 17953−17979.
(46) Perdew, J. P.; Burke, K.; Ernzerhof, M. Generalized Gradient Approximation Made Simple. *Phys. Rev. Lett.* **1996**, *77*, 3865−3868.
(47) Grimme, S. Semiempirical GGA-type density functional constructed with a long-range dispersion correction. *J. Comput. Chem.* **2006**, *27*, 1787−1799.
(48) Schneider, M.; Tang, Z.; Richter, M.; Marschelke, C.; Förster, P.; Wegener, E.; Amin, I.; Zimmermann, H.; Scharnweber, D.; Braun, H.-G.; Luxenhofer, R.; Jordan, R. Patterned Polypeptoid Brushes. *Macromol. Biosci.* **2016**, *16*, 75−81.

https://dx.doi.org/10.1021/acs.langmuir.9b03922
Langmuir 2020, 36, 6828−6836